Elastic differential cross section of *ep* scattering fitted via the differential cross section of *eq* scatterings with cloud-covering effects

Jingle B. Magallanes* and Jinky B. Bornales

Department of Physics, Mindanao State University—Iligan Institute of Technology, Iligan City 9200, Philippines

René Luna-García

Centro de Investigación en Computación, Instituto Politécnico Nacional, Mexico City 07738, Mexico

(Received 26 February 2020; accepted 5 January 2021; published 24 March 2021)

The angular-averaged differential cross section (dcs) of the elastic electron-proton (ep) scattering, covering $Q^2 < 1.0$ GeV^2, was fitted via a combined modified eq-scatterings where q is a point particle. The modifications represent the cloud-covering effects to q. An energy-decaying ratio (edr) was derived by inspecting the generated dcs_{ep} from the form factor data gathered at Mainz Microtron (A1-Collaboration) and Continuous Electron Beam Accelerator Facility (Jefferson Laboratory) when compared to the dcs_{eq} with modified relativistic recoil factor. The diminishing cloud layer, edr, has a decay rate of -2.8 for the datasets under investigation. The formulated spin bare mass (SBM) and spin effective mass (SEM) fitting models use the bare and effective u and d-quark masses, respectively, while spin with other criteria bare mass (SCBM) and spin with other criteria effective mass (SCEM) integrate other considerations. Three comparison methods were used and all of them favor the models with other additional considerations. SCEM was the most favored model in general.

DOI: 10.1103/PhysRevD.103.054032

I. INTRODUCTION

Electron-nucleon scattering has been used to extensively measure the nucleon's electromagnetic form factors to study the charge and magnetization distributions [1]. For this, it is important to measure the scattering's differential cross section (dcs) since it is proportional to the probability for any given reaction or process to occur. The objective of this study is to demonstrate a fitting model to the angular-averaged dcs of the elastic electron-proton (ep) scattering, dcs_{ep}, generated from different form factor datasets covering the transfer momentum, $Q < 1$ GeV.

Initially, it was thought that fitting the dcs_{ep} through electron-point particle (eq) scatterings would be impossible since the proton is definitely not a point particle as characterized by the form factors. However, it could and would be possible by putting some cloud-covering effects on the point particle q. Inasmuch as, at low-energy quantum chromodynamics (QCD) where both perturbation theory and asymptotic freedom are not possible, there are significant collective interactions between the valence and sea quarks; and the effects are in the form of cloud coverings. The valence quarks get surrounded by some dense concentration of virtual quarks and gluons. When probed at low energy, this cloud is the high energy barrier to the core of the proton.

For the range of transfer momenta in consideration, eq-scattering would have to be masked by modifications mantling the particle. This includes the modifications in dcs_{eq}'s recoil factor (fixed cloud layer) and the energy dependent ratio (diminishing cloud layer) between dcs_{ep} and dcs_{eq}.

II. THE ELECTRON-PROTON (EP) SCATTERING

The elastic ep-scattering is one of the fundamental interactions used in the understanding of the structure and the build-up of hadronic physics [2]. It is called Mott or no-structure (ns) scattering when it is the electron that is scattered by the point-particle nucleus. Electrons are very light; with high energies, they can penetrate further into the nucleus. However, they couple to the nuclear magnetic field because they have nonzero spin, an effect carried by the final term in the dcs given in Equation (1). This equation also contains the ratio between the final (E') and initial (E) energies of the electron called the relativistic recoil factor of the nucleon. The cross-section is denoted by σ_{ns} for the Mott scattering:

$$\frac{d\sigma}{d\Omega_{\text{Mott}}} = \sigma_{ns} = \frac{(Z_1 Z_2 \alpha)^2}{4k^2 \sin^4(\frac{\theta}{2})} \left(\frac{E'}{E}\right) \left\{1 - v^2 \sin^2\left(\frac{\theta}{2}\right)\right\} \quad (1)$$

*Also a researcher at Premier Research Institute of Science and Mathematics (PRISM).
jingle.magallanes@g.msuiit.edu.ph; jbmagallanes@gmail.com

where

$$\frac{E'}{E} = \frac{1}{1 + \frac{2E}{M}\sin^2\frac{\theta}{2}} \tag{2}$$

and

$$E - E' = \frac{-\bar{q}^2}{2M} = \frac{Q^2}{2M} \tag{3}$$

with M being the mass of the nucleon. The electron has to release a virtual photon as a necessary condition in order to probe the proton with an energy equal to the difference between the electron's initial and final energies, given by Eq. (3), where $\bar{q}^2$ is the square of the transfer momentum and $-\bar{q}^2 = Q^2$.

Electron scattering has been deeply studied over the years and there are two cases: the elastic scattering characterized by the electromagnetic form factors and the deep inelastic scattering characterized by the structure functions. Electromagnetic form factors of the proton provide some of the first information of its size and distribution of charge and magnetization. Moreover, the observation of unexpected behavior in form factors and structure functions has also brought new understanding of the strong interaction.

The electron being a point-particle has the simple vertex, γ_μ, and its current takes the form $j_\mu = -e\bar{u}(k')\gamma_\mu u(k)$ while the proton has a vertex, Γ^μ, with a current expressed using form factors parametrizing its internal structure. Also, the proton current must be a Lorentz-invariant four-vector that satisfies the parity and current conservation of the electromagnetic interaction. Hence, for a single-photon exchange, two form factors are allowed in the vertex and the current is given by

$$\begin{aligned} J^\mu &= e\bar{v}(p')\Gamma^\mu v(p) \\ &= e\bar{v}(p')\left[F_1(q^2)\gamma^\mu + \frac{i\kappa}{2M}F_2(q^2)\sigma^{\mu\nu}q_\nu\right]v(p) \end{aligned} \tag{4}$$

where $F_1(q^2)$ is the Dirac form factor corresponding to the helicity-conserving current; $F_2(q^2)$ is the Pauli form factor corresponding to the helicity-flip current; $\kappa = 1.793\mu_N$ is the proton anomalous magnetic moment; M is the proton nucleon mass; and $\sigma_{\mu\nu} = 2i[\gamma_\mu, \gamma_\nu]$. For $q^2 \to 0$, $F_1(0) = F_2(0) = 1.0$ in the nonrelativistic limit and the proton is treated as a point-particle where the virtual photon is insensitive to the proton's internal structure.

The dcs becomes

$$\begin{aligned} \frac{d\sigma}{d\Omega} &= \frac{|j_\mu \frac{1}{q^2} J_\mu|^2}{4((k\dot{p})^2 - m^2M^2)}(2\pi)^4\delta^4(k' - k + p - p') \\ &\times \frac{d^3k'd^3p'}{(2\pi)^3 2E'(2\pi)^3 2(M+\omega)}. \end{aligned} \tag{5}$$

where the conservation of momentum is assured by the delta functions. Integrating over the relevant variables; averaging initial spin states; and summing over final ones, the dcs as a function of the scattering angle θ becomes

$$\begin{aligned} \frac{d\sigma}{d\Omega} &= \frac{(Z_1Z_2\alpha)^2}{4k^2\sin^4(\frac{\theta}{2})}\left(\frac{E'}{E}\right)\cos^2\frac{\theta}{2} \\ &\times \left[\left(F_1^2 + \frac{\kappa^2Q^2}{4M^2}F_2^2\right) + \frac{Q^2}{2M^2}(F_1 + \kappa F_2)^2\tan^2\frac{\theta}{2}\right]. \end{aligned} \tag{6}$$

This can simplify to the structureless Mott cross section multiplied with the form factor term where $(1 - v^2\sin^2\frac{\theta}{2}) \to \cos^2\frac{\theta}{2}$, for relativistic electrons. If the proton were a point charge, its dcs would have only been

$$\frac{d\sigma}{d\Omega} = \frac{(Z_1Z_2\alpha)^2}{4k^2\sin^4(\frac{\theta}{2})}\left(\frac{E'}{E}\right)\left[\cos^2\frac{\theta}{2} + \frac{Q^2}{2M^2}\sin^2\frac{\theta}{2}\right]. \tag{7}$$

To avoid the interference between F_1 and F_2 in Eq. (6), the structure-dependent part of the cross section can be rewritten in terms of the electric and magnetic form factors $G_E(Q^2)$ and $G_M(Q^2)$ [3] where $G_E(Q^2) = F_1(Q^2) - \kappa\tau F_2(Q^2)$ and $G_M(Q^2) = F_1(Q^2) + \kappa F_2(Q^2)$. Then, with $\tau = Q^2/4M^2$, the dcs becomes

$$\frac{d\sigma}{d\Omega} = \frac{(Z_1Z_2\alpha)^2}{4k^2\sin^4(\frac{\theta}{2})}\left(\frac{E'}{E}\right)\cos^2\frac{\theta}{2} \times \left[\frac{G_E^2 + \tau G_M^2}{1+\tau} + 2\tau G_M^2\tan^2\frac{\theta}{2}\right] \tag{8}$$

which can be further simplified to

$$\frac{d\sigma}{d\Omega} = \sigma_{ns}\frac{1}{1+\tau}\left[G_E^2 + \frac{\tau}{\epsilon}G_M^2\right] \tag{9}$$

where

$$\begin{aligned} 1/\epsilon &= [1 + 2(1 + Q^2/4M^2)\tan^2(\theta/2)] \\ &= [1 + 2(1+\tau)\tan^2(\theta/2)]; \end{aligned} \tag{10}$$

ϵ is an angular variable. In the nonrelativistic limit, $Q \to 0$, these form factors are just the Fourier transforms of the charge and magnetization distributions [4],

$$F_{nr}(Q^2) = \int \rho(\vec{r})e^{-\vec{Q}\cdot\vec{r}}d^3\vec{r}. \tag{11}$$

Dipole form factor,

$$G_D(Q^2) = \frac{1}{(1 + a^2Q^2)^2} \tag{12}$$

comes out if the charge distribution is exponential, $\rho(r) = \rho_0 e^{-r/a}$, where a is the scale of the proton radius

given by $a^2 = (0.71\ \mathrm{GeV}^2)^{-1}$. If the charge and magnetic moment distributions are the same, then their transforms will be as well; and generally, the form factor ratio will be

$$\frac{\mu G_E(Q^2)}{G_M(Q^2)} = 1.0, \tag{13}$$

which is known as the form factor scaling. For low Q^2, at which the electric and magnetic root mean square (rms) radii can be determined [5], the form factors can be expanded as

$$\frac{G(Q^2)}{G(0)} = 1 - \frac{1}{6}\langle r^2\rangle Q^2 + \frac{1}{120}\langle r^4\rangle Q^4 - \cdots. \tag{14}$$

The (rms) radius can be determined from the slope of the form factors at $Q^2 = 0$ with

$$\langle r^2\rangle = -\frac{6}{G(0)}\frac{dG(Q^2)}{dQ^2}\bigg|_{Q^2=0}. \tag{15}$$

III. LOW ENERGY FORM FACTOR DATA

Form factors can be extracted via the Rosenbluth extraction method [6–8]. The form factor ratio $\frac{\mu G_E}{G_M}$ is ~1.0 at lower energies with the world data in [7,9–12] and this is consistent with the form factor scaling. Other methods of extractions are the polarization transfer method [13] and super-Rosenbluth method [14]. Previous Rosenbluth data used the Bosted global fit [15] valid at $0 < Q^2 < 7\ \mathrm{GeV}^2$. Recently, the global fitting procedure [1,16] was used for the world data valid for Q^2 up to ~30 GeV^2. There was already an attempt in separating the quark flavor contributions to the elastic form factors at low-energy, detailed in [17].

The low momentum transfer data presented in [18,19] were determined from the measurements at the Mainz Microtron (MAMI) using the 3-spectrometer-facility of the A1-Collaboration taken in three periods between 2006 and 2007 using beam energies of 180, 315, 450, 585, 720, and 855 MeV. The experiment covers $0.004\ \mathrm{GeV}^2 < Q^2 < 1.0\ \mathrm{GeV}^2$ with counting rate uncertainties below 0.2% for most of the data points [5]. They separate the form factors by fitting a wide selection of models directly to the measured cross sections. Extensive simulations were done to test the validity of this method. Standard Rosenbluth extraction technique was used in comparing the results. Form factors determined via Rosenbluth separation method, Friedrich-Walcher model, polynomial model and spline model were used in this study. The details pertaining to the measurements and analyses can be found in [19].

For the experiment presented in [8], high-precision proton Rosenbluth extractions using beam energies from 849 MeV to 5.157 GeV were performed covering a large range of transfer momenta, $0.40\ \mathrm{GeV}^2 < Q^2 < 5.76\ \mathrm{GeV}^2$, focusing on the extremes of ϵ where two-photon exchanges (TPEs) occur. The experiment has higher momentum transfers than proton Rosenbluth experiments before this and provided higher precision at low momentum transfer. To reconcile the discrepancy of results with that of Polarization data, considerations were taken including the missing corrections from TPE, which are difficult to calculate, and the results from other experiments but are not expected to be valid at low Q^2. But for this study, only $Q^2 < 1\ \mathrm{GeV}^2$ were considered and in which case TPE rarely happens, hence, correction will be not as reliable. For the purposes of comparing the models with the available data, only some of the Rosenbluth extracted values were included. The details pertaining to the experiment and data analyses are found in [8].

IV. IMPLEMENTATIONS

The averaged multiple-angle dcs_{ep} was fitted by the modified dcs of eq-scatterings at transfer momenta less than 1 GeV where q is a point particle. Since the proton is a finite particle, cloud-covering effects have to be carried-out on q. This also warrants that $m_q < m_p$, in terms of particle masses. The quark flavor composition of the proton (uud) was the basis in the choice of masses for the q's in the fitting models; taking the quark masses and their corresponding fractional charges. Accordingly, effective (low energy) quark masses [20,21] are assigned to q for the transfer momentum in consideration, but it could also be assigned bare quark masses [20,22] since the cloud-effect is already represented by the modifications. The relativistic recoil factor of the angle and spin averaged dcs of eq-scattering was modified using the proton mass as a parameter. Overlapping of the electron wave functions, spin-spin interactions, and color interactions were also considered in coming-up with the fitting models but arbitrarily not quantitative yet. The form factors derived from experiments at Mainz Microtron (MAMI) [18,19] and Continuous Electron Beam Accelerator Facility (CEBAF, JLab) [8] were used to generate the data for dcs_{ep}.

The angular-averaged dcs_{ep} were generated via Eq. (8) in ROOT Data Analysis Framework [23] platform. Raw dcs of eq-scattering with q having the mass of u-quark (dcs_{eu}) and d-quark (dcs_{ed}) were also simultaneously generated using the same random numbers via Eq. (7). A total of 2000 data points each for dcs_{ep}, dcs_{eu}, and dcs_{ed} were gathered at random various scattering angles from 0° to 180° for each corresponding particular transfer momentum in the experimental data considered. The energy-decaying ratios, which decreases as photon energy increases, between dcs_{ep} and dcs_{eq} were then determined and incorporated back to the dcs_{eq} modifying them further. New data points were generated and then reanalyzed.

Equation (2) is the relativistic recoil factor and this is due to the recoil of the target particle during the interaction [4,24].

TABLE I. Energy-decaying ratio: The edr was derived from the comparison of the data gathered by the known method of extracting form factors at low transfer momentum (Rosenbluth Extraction Method) to the dcs_{eu} and dcs_{ed} at fixed transfer momentum.

Form factor datasets	A	r	Form	Notation
Rosenbluth separation data [19] ep-eu with bare mass	3.50	2.8	$3.50e^{-2.8Q^2}$	edr_{ubs}
Rosenbluth separation data [19] ep-ed with bare mass	14.0	2.8	$14.0e^{-2.8Q^2}$	edr_{dbs}
Rosenbluth separation data [19] ep-eu with effective mass	2.40	2.8	$2.40e^{-2.8Q^2}$	edr_{ues}
Rosenbluth separation data [19] ep-ed with effective mass	9.60	2.8	$9.60e^{-2.8Q^2}$	edr_{des}
Rosenbluth extraction data [8] ep-eu with bare mass	1.85	1.8	$1.85e^{-1.8Q^2}$	edr_{ube}
Rosenbluth extraction data [8] ep-ed with bare mass	7.40	1.8	$7.40e^{-1.8Q^2}$	edr_{dbe}
Rosenbluth extraction data [8] ep-eu with effective mass	1.45	1.8	$1.45e^{-1.8Q^2}$	edr_{uee}
Rosenbluth extraction data [8] ep-ed with effective mass	5.80	1.8	$5.80e^{-1.8Q^2}$	edr_{dee}

Its modification has a significant change to the dcs, acting like a fixed layer of cloud, as it shifts the dcs_{eq} distribution vertically and closer to the dcs_{ep} when the mass used is similar to that of proton. At a particular Q^2 and considering an angle-averaged dcs, the recoil factor is a constant. This materializes the proton mass as a parameter to the fitting model.

Correspondingly, the averaged points in the same transfer momentum for dcs_{ep} and dcs_{eq} were compared. There is a decreasing ratio, between dcs_{ep} and dcs_{eu} and more so with dcs_{ed}, behaving exponentially. A dimensionless energy-decaying ratio (edr) of the form Ae^{-rQ^2} was found for the investigated Rosenbluth form factor datasets with A as the amplitude and r as the decay rate, see Table I. There are differences in the amplitudes of the edr_{d**} and edr_{u**} but the decay rate for each dataset is the same. It should be noted that the dataset from [19] has 27 selected data points while [8] only has 6 data points; experiments from which the datasets were taken have different considerations.

Combined fitting models with contributions from both dcs_{eu} and dcs_{ed} underpins the quark flavor composition of the proton. Additionally, the weight of the modified dcs_{eu} and dcs_{ed} contributions can be affected by the overlapping of the electron's initial and final wave functions, spin-spin interactions of the electron and proton, and color interactions of the quarks inside the proton, and other considerations. For instance, the contributions can be arbitrarily set to be 80% instead of $2/3$ for dcs_{eu} and 20% instead of $1/3$ for dcs_{ed}.

V. RESULTS

When probed with very low energy, most if not all, hadrons are just point particles. Gradual increase in the probe energy reveals that they are actually extended particles. At low energy, the valence quarks are cloud covered constituent quarks and the proton would be a lump of clouds with an extended size. And, it is difficult to describe this lump without increasing the energy of the photon probe. The cloud, however, can be treated as an energy barrier through the core of the proton which can be diminished by increasing the energy probe.

Table I tabulates the edr for the Rosenbluth datasets [8,19]. The amplitudes of the edr were derived by separately comparing dcs_{eu} and dcs_{ed} to dcs_{ep}. Compromising results of point to point comparison, corresponding to different transfer momenta, led to a consensus amplitude ratio of ~4. One of the critical reasons being looked into is that, at very low transfer momenta, the ratio between dcs_{eu} and dcs_{ed} is predominantly affected by the ratio of the squares of their respective charges. Thus, in order to close-in with dcs_{ep}, dcs_{ed} have to be intensified by about four times as much as dcs_{eu}. However, the transfer momentum, as it increments, also eventually affects the dcs ratio in addition to the effects contributed by the assigned masses to the point particles; this aspect is open for more investigations. Moreover, the amplitudes for edr_{*e*} are lesser than edr_{*b*} since, at the range of transfer momenta in consideration, the particles with effective masses are presumably having thinner clouds than those carrying their bare masses. The decay rate of the diminishing cloud effect layer, edr, for each dataset is constant. It can be seen, however, that the decay rate for Rosenbluth form factor in [19] is greater than in [8]. The reason for this is speculated to be caused by either or both the experimental setup considerations and of the statistical data size.

The dcs_{ep} generated from the investigated Rosenbluth form factor datasets are compared to the $edr_{u**}dcs_{eu}$ and $edr_{d**}dcs_{ed}$ and three ways of comparison were done—ratio test (averaging the ratios between the corresponding generated experimental data and fitting data) in Table II, absolute difference (averaging the absolute differences between the corresponding generated experimental data and fitting data) in Table III and chi test (square-root of the average of the squares of the differences between the corresponding generated experimental data and fitting data) in Table IV. Other form factor datasets were also used for comparison such as those determined by Friedrich-Walcher, Polynomial and Spline models with 68.3% confidence level. The description of the other form factor

TABLE II. Ratio test: the average ratio between the dcs_{ep} generated from the different datasets to their corresponding dcs_{eu} and dcs_{ed} with edr where bare quark masses (BM) are used and, separately, for effective quark masses (EM).

Form factor datasets	ep-eu (BM)	ep-ed (BM)	ep-eu (EM)	ep-ed (EM)
Rosenbluth extraction [8]	0.96964	0.96971	1.0003	0.99732
Rosenbluth separation [19]	1.0167	1.0173	0.98951	0.98742
Friedrich-Walcher model [19]	1.0504	1.0507	1.1520	1.1490
Polynomial model [19]	1.2053	1.2056	1.3455	1.3420
Spline model [19]	1.2134	1.2138	1.3558	1.3521

TABLE III. Absolute difference: the average absolute difference between the dcs_{ep} generated from the different datasets and their corresponding dcs_{eu} and dcs_{ed} with edr where bare quark masses (BM) are used and, separately, for the effective quark masses (EM).

Form factor datasets	ep-eu (BM) $\times 10^{-6}$	ep-ed (BM) $\times 10^{-6}$	ep-eu (EM) $\times 10^{-6}$	ep-ed (EM) $\times 10^{-6}$
Rosenbluth extraction [8]	6.6196	6.6253	2.3954	2.1956
Rosenbluth separation [19]	832.92	841.93	225.39	238.93
Friedrich-Walcher model [19]	737.26	744.84	197.24	204.42
Polynomial model [19]	738.73	746.31	204.99	212.17
Spline model [19]	739.24	746.80	204.82	211.86

TABLE IV. Chi test: the chi test between the dcs_{ep} generated from the different datasets from their corresponding dcs_{eu} and dcs_{ed} with edr where bare quark masses (BM) are used and, separately, for effective quark masses (EM).

Form factor datasets	ep-eu (BM) $\times 10^{-6}$	ep-ed (BM) $\times 10^{-6}$	ep-eu (EM) $\times 10^{-6}$	ep-ed (EM) $\times 10^{-6}$
Rosenbluth extraction [8]	8.9374	8.9499	4.2973	3.8496
Rosenbluth separation [19]	1647.3	1666.2	375.85	394.87
Friedrich-Walcher model [19]	2565.1	2591.5	603.56	619.44
Polynomial model [19]	2557.6	2584.0	611.84	627.73
Spline model [19]	2558.0	2584.1	612.10	627.25

models and the parameters for their best fits are found in chapter 7 and Appendix J of [19].

For the ratio test in Table II, the dcs_{ep} generated from form factors of the models from [19] were closer to the modified dcs_{eu}, except for the Rosenbluth extraction data of [8], than to the modified dcs_{ed} where the q's assume bare masses. As expected, the dcs_{ep} generated from Rosenbluth extraction method are the ones closer to $edr_{u**}dcs_{eu}$ and $edr_{d**}dcs_{ed}$ compared to the ones generated from other datasets. However, corresponding numbers as seen in Table II are not in agreement among themselves which could be attributed to the differences in the experimental set-ups from which the two datasets were taken. The data from [19] were derived from the set-up that was intended for measurements using low beam energies while from [8] were measured from the setup intended for higher beam energies.

For the absolute difference in Table III, the dcs_{ep} generated from different datasets were more in agreement with $edr_{*e*}dcs_{e*}$ than $edr_{*b*}dcs_{e*}$ since the differences are much smaller in favor of the dcs where quarks are assuming the effective masses. It can also be seen that all the dcs_{ep} are in more agreement with $edr_{u**}dcs_{eu}$ than with $edr_{d**}dcs_{ed}$ except for the Rosenbluth extraction data [8]. Among the datasets from [19], the generated dcs_{ep} from Friedrich-Walcher has the lowest average absolute difference.

For the chi test in Table IV, the dcs_{ep} generated from different datasets were more in agreement with $edr_{*e*}dcs_{e*}$ than $edr_{*b*}dcs_{e*}$ since the deviation are much smaller in favor of the dcs where the point particles assume effective quark masses. Again, it can also be seen that all the dcs_{ep} are in more agreement with $edr_{u**}dcs_{eu}$ than with $edr_{d**}dcs_{ed}$ except for the Rosenbluth extraction data [8]. Expectedly, among the datasets from [19], the generated dcs_{ep} from Rosenbluth separation data is the most favored by the chi test.

Considering Eq. (7), edr, weight contribution by quark flavor composition and, additionally, other criteria, four fitting models were formulated (see Table V). The first is the spin bare mass (SBM) which takes into account the respective contributions of edr_{*bs} and dcs_{e*}. Second, is the spin with other criteria bare mass (SCBM) which is just the SBM but including the other considerations. The third is the spin effective mass (SEM) which has lower amplitudes compared to the SBM and uses the effective quark masses. The fourth one, spin with other criteria effective mass (SCEM), is just the SEM but considering the same other criteria included in SCBM.

TABLE V. The dcs_{eq} models: the four models include SBM, SCBM, SEM, and SCEM and their forms.

Model	Form
Spin bare mass (SBM)	$(2/3)3.50e^{-2.8Q^2}dcs_{eu} + (1/3)14.0e^{-2.8Q^2}dcs_{ed}$
Spin with other criteria bare mass (SCBM)	$(4/5)3.50e^{-2.8Q^2}dcs_{eu} + (1/5)14.0e^{-2.8Q^2}dcs_{ed}$
Spin effective mass (SEM)	$(2/3)2.40e^{-2.8Q^2}dcs_{eu} + (1/3)9.60e^{-2.8Q^2}dcs_{ed}$
Spin with other criteria effective mass (SCEM)	$(4/5)2.40e^{-2.8Q^2}dcs_{eu} + (1/5)9.60e^{-2.8Q^2}dcs_{ed}$

TABLE VI. Ratio test: the average ratio between the dcs_{ep} of the different datasets to their corresponding dcs_{eq} of the different models.

Form factor datasets	SBM	SCBM	SEM	SCEM
Rosenbluth extraction [8]	0.96967	0.96966	0.99933	0.99973
Rosenbluth separation [19]	1.0169	1.0168	0.98881	0.98909
Friedrich-Walcher model [19]	1.0505	1.0505	1.1510	1.1514
Polynomial model [19]	1.2054	1.2053	1.3443	1.3448
Spline model [19]	1.2135	1.2135	1.3546	1.3550

TABLE VII. Absolute difference: the average absolute difference between the dcs_{ep} of the different datasets and their corresponding dcs_{eq} of the different models|spin bare mass (SBM), spin with other criteria bare mass (SCBM), spin effective mass (SEM) and spin with other criteria effective mass (SCEM).

Form factor datasets	SBM $\times 10^{-6}$	SCBM $\times 10^{-6}$	SEM $\times 10^{-6}$	SCEM $\times 10^{-6}$
Rosenbluth extraction [8]	6.6215	6.6207	2.3035	2.3403
Rosenbluth separation [19]	835.92	834.72	229.90	228.09
Friedrich-Walcher model [19]	739.79	738.78	199.64	198.68
Polynomial model [19]	741.26	740.25	207.38	206.42
Spline model [19]	741.76	740.76	207.16	206.22

The ratio test in Table VI, absolute difference in Table VII and chi test in Table VIII show the comparisons of the data between the four fitting models and the corresponding generated dcs_{ep} from different form factor datasets listed. The plots of the dcs_{ep} from the Rosenbluth datasets with all the four models almost lie on the same space. It can be seen in Table VI that, in general, the dcs_{ep}'s are in agreement with SCBM for the ratio test. On the other hand, both dcs_{ep}'s from the Rosenbluth form factor datasets are in close agreement with SCEM.

For the comparison using absolute difference in Table VII, SCBM is favored over SBM by all the generated dcs_{ep} from different form factor datasets. In general, SCEM is also favored by the generated dcs_{ep} except those generated from Rosenbluth extraction data from [8] and this could be due to the experimental parameters in considerations. With the numbers given in this table, the SCEM is most favored since its corresponding average absolute difference is smaller compared to SCBM; both fitting models feature the other additional criteria.

TABLE VIII. Chi test: the chi test between the dcs_{ep} of the different datasets and their corresponding dcs_{eq} of the different models| spin bare mass (SBM), spin with other criteria bare mass (SCBM), spin effective mass (SEM) and spin with other criteria effective mass (SCEM).

Form factor datasets	SBM $\times 10^{-6}$	SCBM $\times 10^{-6}$	SEM $\times 10^{-6}$	SCEM $\times 10^{-6}$
Rosenbluth extraction [8]	8.9416	8.9399	4.1442	4.2050
Rosenbluth separation [19]	1653.6	1651.1	382.19	379.65
Friedrich-Walcher model [19]	2573.9	2570.4	608.85	606.73
Polynomial model [19]	2566.4	2562.9	617.13	615.01
Spline model [19]	2566.7	2563.2	617.14	615.13

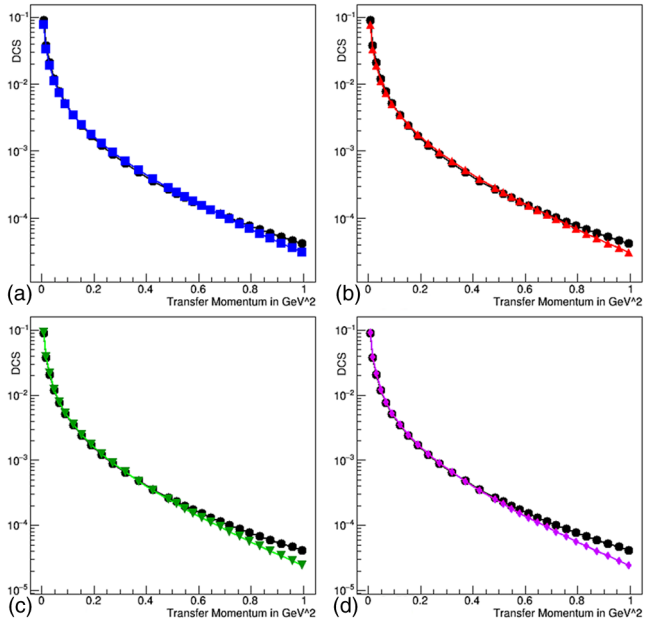

FIG. 1. The plot shows the generated dcs_{ep} (black circle) using the form factors from Friedrich-Walcher model [19] versus Q^2. They were compared to (a) dcs_{SBM} (black square), (b) dcs_{SCBM} (black up-pointing triangle), (c) dcs_{SEM} (black down-pointing triangle), and (d) dcs_{SCEM} (black diamond suit), showing a pronounced agreement.

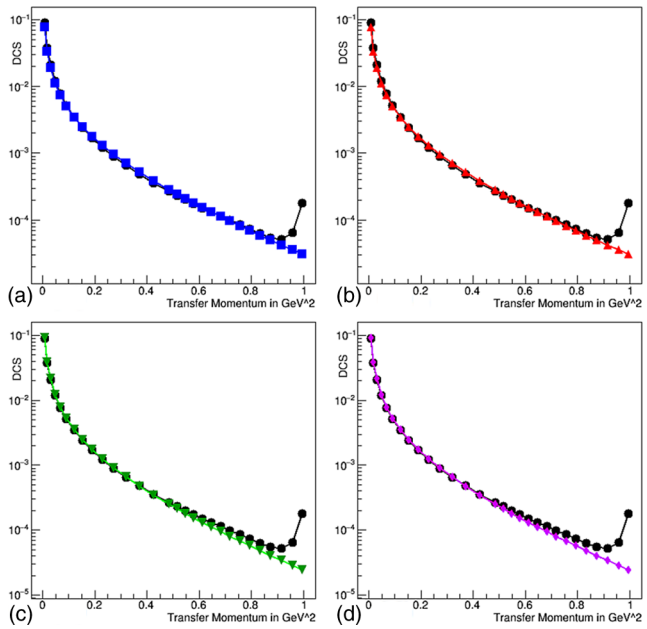

FIG. 2. The plot shows the generated dcs_{ep} (black) using the form factors from spline model [19] versus Q^2. They were compared to (a) dcs_{SBM} (black square), (b) dcs_{SCBM} (black up-pointing triangle), (c) dcs_{SEM} (black down-pointing triangle), and (d) dcs_{SCEM} (black diamond suit), showing good agreement except with the two points at the tail.

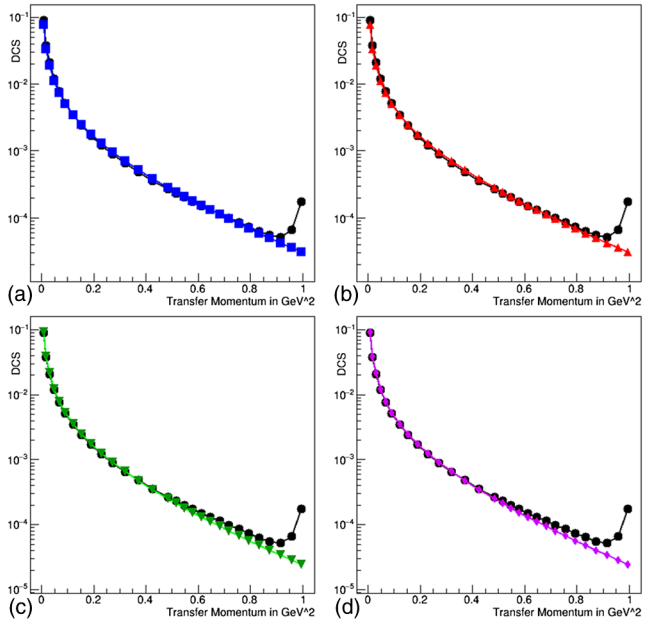

FIG. 3. The plot shows the generated dcs_{ep} (black) using the form factors from polynomial model [19] versus Q^2. They were compared to (a) dcs_{SBM} (black square), (b) dcs_{SCBM} (black up-pointing triangle), (c) dcs_{SEM} (black down-pointing triangle), and (d) dcs_{SCEM} (black diamond suit), showing good agreement except with the two points at the tail.

The plots in Figs. 1, 2, and 3 show the dcs_{ep} of form factors derived from Friedrich-Walcher, spline and polynomial models, respectively, together with the formulated fitting models. From these three datasets, it is the generated dcs_{ep} from the Friedrich-Walcher form factors that has the smallest average absolute difference. Looking at Figs. 2 and 3, it can be seen that the last two data points from the datasets diverge way off from the models and this could be attributed by the limitations of the experimental setup and the fitting parameters when the form factors were derived. It is also only up to this region that the formulated fitting models are expected to be valid.

For the comparison using chi test in Table VIII, it is expected that the Rosenbluth form factor datasets are favorable to all four models since the chi test values are smaller, compared to the other datasets; but more specially to SCBM and SCEM. With general considerations, it is the SCEM that is the most favored model for this comparison test with SEM coming next.

VI. CONCLUSIONS AND RECOMMENDATIONS

Several experimental data, such as those coming from A1-Collaboration and JLab, have measured the proton electromagnetic form factors with precision and accuracy for relativistic systems through elastic scatterings. These measurements, specially for $Q^2 < 1$ GeV^2, are important since they give the electric and magnetic form factors that

determine the distribution of charge and magnetization of the proton or its charge and magnetic (rms) radii.

The dcs_{ep} generated from different sets of form factor data were compared to raw dcs_{eq} where q is a point particle assigned with bare and effective masses of u and d quarks. The edr's were determined from this comparison and are listed in Table I. The edr that suit best the generated data corresponds to the one derived from Rosenbluth separation data in [19]. The amplitude of edr_{d**} is greater than that of edr_{u**} and this is due to their differences in charge and, eventually, in mass as transfer momentum increments. It is recommended that this will be delved more; specially, on the behavior of the ratio edr_{d**}/edr_{u**}. Also, $edr_{*e*} < edr_{*b*}$ and this could be due to the dominance of the constituent or effective mass at the range of transfer momentum studied. Aside from that, it is quite logical that the point particle with (smaller) bare mass would need a thicker cloud to compensate for its mass compared to the one with (bigger) effective mass. The decay rate in the edr is constant, however, this could change depending on the number of data points considered in the formulation of the fitting model or if different form factor datasets are used, in addition to the speculation that this variation could also be due to the differences in the setup and parameters considered in the experiments; as can be seen, $edr_{**s} > edr_{**e}$. By averaging the dcs of 2000 events, each taken with different and randomly selected scattering angles from 0° to 180°, the recoil factor can be treated as a constant. Moreover, it was necessary to modify the recoil factor of the eq-scattering by using the proton mass to shift the distribution of dcs_{eq} closer to dcs_{ep}. And, this materializes the proton as a parameter to the fitting model. The existence of the edr and the modification of the recoil factors, foremost, are acting as the cloud layers that are supposed to cover the point particle q at low energy. Furthermore, Tables II, III, and IV imply with generality that the generated dcs_{ep} favors $edr_{u**}dcs_{eu}$ over $edr_{d**}dcs_{ed}$.

Four models were formulated (see Table V) considering the assignment of bare and effective quark masses—SBM and SEM consider the edr and contributions based on the quark flavor composition of the proton while SCBM and SCEM incorporate other considerations, albeit arbitrarily, such as overlapping of the electron wave functions, spin-spin interactions, and color interactions. For the ratio test, SCBM is the most favored model while SCEM is favored by both the absolute difference and chi test. With SCEM and SEM having favorable comparative numbers imply that at this range of transfer momenta, the said models are consistent on the point particles being likely to assume effective masses rather than bare masses. It should be noted that the fitting models are not meant to prove the quark composition of the proton but, rather, show that previous and known results of eq-scattering with modifications can be used to create models for ep-scattering at low transfer momenta.

Although the additional arbitrary considerations has an effect to the elastic ep-scattering, it is assumed to be really very small in magnitude for $Q^2 < 1$ GeV^2 but its existence in the models have been very helpful in optimizing the comparison tests as manifested by both the SCBM and SCEM models. It is recommended, for example, to reassess the geometrical arrangement preferences of the quarks and gluons and the configuration counting in order to have a more optimized fitting model. Variations in the results are also expected by considering more number of events and thus involving more scattering angles. The cloud covering is also affected by the overlapping of the electron's initial and final wave functions and the overall spin-spin interactions between the electron and proton. These effects will be investigated more.

ACKNOWLEDGMENTS

The Mindanao State University—Iligan Institute of Technology (MSU-IIT) and its Department of Physics and the Premier Research Institute of Science and Mathematics (PRISM) of Iligan City, Philippines; Research Center for Theoretical Physics (RCTP) of Jagna, Philippines; and Centro de Investigacion en Computacion—Instituto Politecnico Nacional (CIC-IPN) of CDMX, Mexico are acknowledged for their conducive venues in making this research possible. Gratitude is extended to the Department of Science and Technology (DOST) of the Philippines and MSU-IIT for their financial support. The inspiration and encouragements from Prof. Christopher Bernido, Prof. Maria Victoria Bernido, Prof. Ludwig Streit, and Prof. Roland Winkler are highly appreciated.

[1] Z. Ye, J. Arrington, R. J. Hill, and G. Lee, Proton and neutron electromagnetic form factors and uncertainties, Phys. Lett. B **777**, 8 (2018).

[2] J. Dainton, The structure of hadronic physics, Physikalische Blätter **55-7/8**, 75 (1999).

[3] R. G. Sachs, High-energy behavior of nucleon electromagnetic form factors, Phys. Rev. **126**, 2256 (1962).

[4] F. Halzen and A. D. Martin, *Quarks and Leptons: An Introductory Course in Modern Particle Physics* (John Wiley and Sons, Incorporated, New York, 1984).

[5] J. C. Bernauer *et al.*, High-Precision Determination of the Electric and Magnetic form Factors of the Proton, Phys. Rev. Lett. **105**, 242001 (2010).
[6] M. N. Rosenbluth, High energy elastic scattering of electrons on protons, Phys. Rev. **79**, 615 (1950).
[7] C. Berger, V. Burkert, G. Knop, B. Langenbeck, and K. Rith, Electromagnetic form factors of the proton at squared four-momentum transfers between 10 and 50 fm^{-2}, Phys. Lett. **35B**, 87 (1971).
[8] M. J. Johnson, Two-photon exchange effects in elastic electron-proton scattering, Ph.D Dissertation, Northwestern University, Illinois, USA, 2013, https://doi.org/10.2172/1093450.
[9] L. Andivahis *et al.*, Measurements of the electric and magnetic form factors of the proton from $Q^2 = 1.75$ to $8.83(\mathrm{GeV}/c)^2$, Phys. Rev. D **50**, 5491 (1994).
[10] R. C. Walker *et al.*, Measurements of the proton elastic form factors for $1 \leq Q^2 \leq 3(\mathrm{GeV}/c)^2$ at SLAC, Phys. Rev. D **49**, 5671 (1994).
[11] T. Janssens, R. Hofstadter, E. B. Hughes, and M. R. Yearian, Proton form factors from elastic electron-proton scattering, Phys. Rev. **142**, 922 (1966).
[12] J. Litt *et al.*, Measurement of the ratio of the proton form factors, G_E/G_M, at high momentum transfers and the question of scaling, Phys. Lett. **31B**, 40 (1970).
[13] M. Jones *et al.*, G_{E_p}/G_{M_p} Ratio by Polarization Transfer in $ep \to ep$, Phys. Rev. Lett. **84**, 1398 (2000).
[14] I. A. Qattan *et al.*, Precision Rosenbluth Measurement of the Proton Elastic form Factors, Phys. Rev. Lett. **94**, 142301 (2005).
[15] P. E. Bosted, Empirical fit to the nucleon electromagnetic form factors, Phys. Rev. C **51**, 409 (1995).
[16] G. Lee, J. R. Arrington, and R. J. Hill, Extraction of the proton radius from electron-proton scattering data, Phys. Rev. D **92**, 013013 (2015).
[17] G. D. Cates, C. W. de Jager, S. Riordan, and B. Wojtsekhowski, Flavor Decomposition of the Elastic Nucleon Electromagnetic form Factors, Phys. Rev. Lett. **106**, 252003 (2011).
[18] J. C. Bernauer, Precise form factors from elastic electron scattering, J. Phys. **381**, 012006 (2012).
[19] J. C. Bernauer, Measurement of the elastic electron-proton cross section and separation of the electric and magnetic form factor in the Q^2 range from 0.004 to 1 $(\mathrm{GeV}/c)^2$, (United States Department of Energy, Office of Scientific and Technical Information: 21403504), Ph.D. Dissertation, Mainz University, Germany, 2010.
[20] W. M. Yao *et al.*, Review of particle physics (Particle physics booklet), J. Phys. G **33**, 1 (2006).
[21] D. J. Griffiths, *Introduction to Elementary Particles* (WILEY-VCH, Weinheim, 2008).
[22] C. Patrignani *et al.* (Particle Data Group), Review of particle physics, Chin. Phys. C **40**, 100001 (2016).
[23] R. Brun and F. Rademakers, ROOT—An object oriented data analysis framework, Nucl. Instrum. Methods Phys. Res., Sect. A **389**, 81 (1997); See also http://root.cern.ch (1997).
[24] V. J. Martin, Lectures on Particle Physics (University of Edinburgh, Edinburgh, Scotland, 2012), https://www2.ph.edu.ac.uk/∼vjm.